Plasmon-induced transparency with detuned ultracompact Fabry-Perot resonators in integrated plasmonic devices

Zhanghua Han* and Sergey I. Bozhevolnyi

Institute of Sensors, Signals and Electrotechnics (SENSE), University of Southern Denmark, Niels Bohrs Alle 1, DK-5230 Odense M, Denmark

**zhh@sense.sdu.dk*

Abstract: We demonstrate the realization of on-chip plasmonic analogue of electromagnetically induced transparency (EIT) in integrated plasmonic devices using detuned Fabry-Perot resonators aperture-side-coupled to a metal-insulator-metal (MIM) waveguide, with the transmission peak occurring at the intermediate wavelength. Strong MIM mode confinement along with localized side-coupling allows one to realize subwavelength photonic components with EIT-like transmission. Numerical results show that MIM components exhibiting pronounced EIT-like spectra in near infrared with the footprint of < 0.15 μm^2 and group index of ~26 can be designed.

OCIS codes: (240.6680) Surface plasmons; (160.3918) Metamaterials

References and links

1. K.-J. Boller, A. Imamolu, and S. Harris, "Observation of electromagnetically induced transparency," Phys. Rev. Lett. **66**(20), 2593–2596 (1991).
2. D. D. Smith, H. Chang, K. A. Fuller, A. T. Rosenberger, and R. W. Boyd, "Coupled resonator induced transparency," Phys. Rev. A **69**(6), 063804 (2004).
3. Q. Xu, S. Sandhu, M. L. Povinelli, J. Shakya, S. Fan, and M. Lipson, "Experimental realization of an on-chip all-optical analogue to electromagnetically induced transparency," Phys. Rev. Lett. **96**(12), 123901 (2006).
4. S. Zhang, D. A. Genov, Y. Wang, M. Liu, and X. Zhang, "Plasmon-induced transparency in metamaterials," Phys. Rev. Lett. **101**(4), 047401 (2008).
5. N. Liu, T. Weiss, M. Mesch, L. Langguth, U. Eigenthaler, M. Hirscher, C. Sönnichsen, and H. Giessen, "Planar metamaterial analogue of electromagnetically induced transparency for plasmonic sensing," Nano Lett. **10**(4), 1103–1107 (2010).
6. R. D. Kekatpure, E. S. Barnard, W. Cai, and M. L. Brongersma, "Phase-coupled plasmon induced transparency," Phys. Rev. Lett. **104**(24), 243902 (2010).
7. M. Fleischhauer, A. Imamoglu, and J. P. Marangos, "Electromagnetically induced transparency: Optics in coherent media," Rev. Mod. Phys. **77**(2), 633–673 (2005).
8. S. I. Bozhevolnyi, A. B. Evlyukhin, A. Pors, M. G. Nielsen, M. Willatzen, and O. Albrektsen, "Optical transparency by detuned electrical dipoles," N. J. Phys. in press.
9. S. I. Bozhevolnyi, "Effective-index modeling of channel plasmon polaritons," Opt. Express **14**(20), 9467–9476 (2006), http://www.opticsinfobase.org/abstract.cfm?URI=oe-14-20-9467.
10. S. I. Bozhevolnyi, V. S. Volkov, E. Devaux, J.-Y. Laluet, and T. W. Ebbesen, "Channel plasmon subwavelength waveguide components including interferometers and ring resonators," Nature **440**(7083), 508–511 (2006).
11. Z. Han, A. Y. Elezzabi, and V. Van, "Experimental realization of subwavelength plasmonic slot waveguides on a silicon platform," Opt. Lett. **35**(4), 502–504 (2010).
12. S. I. Bozhevolnyi, and J. Jung, "Scaling for gap plasmon based waveguides," Opt. Express **16**(4), 2676–2679 (2008), http://www.opticsinfobase.org/oe/abstract.cfm?URI=oe-16-4-2676.
13. Z. Han, "Ultracompact plasmonic racetrack resonators in metal-insulator-metal waveguides," Photonics and Nanostructures-Fundamentals and Applications **8**(3), 172–176 (2010).
14. Z. Han, V. Van, W. N. Herman, and P.-T. Ho, "Aperture-coupled MIM plasmonic ring resonators with sub-diffraction modal volumes," Opt. Express **17**(15), 12678–12684 (2009), http://www.opticsinfobase.org/abstract.cfm?URI=oe-17-15-12678.
15. P. Johnson, and R. Christy, "Optical constants of the noble metals," Phys. Rev. B **6**(12), 4370–4379 (1972).
16. A. B. Evlyukhin, S. I. Bozhevolnyi, A. Pors, M. G. Nielsen, I. P. Radko, M. Willatzen, and O. Albrektsen, "Detuned electrical dipoles for plasmonic sensing," Nano Lett. **10**(11), 4571–4577 (2010).

#140919 - $15.00 USD Received 10 Jan 2011; revised 26 Jan 2011; accepted 30 Jan 2011; published 3 Feb 2011

17. J. B. Khurgin, and P. A. Morton, "Tunable wideband optical delay line based on balanced coupled resonator structures," Opt. Lett. **34**(17), 2655–2657 (2009).
18. Y. Zhang, S. Darmawan, L. Y. M. Tobing, T. Mei, and D. H. Zhang, "Coupled resonator-induced transparency in ring-bus-ring Mach-Zehnder interferometer," J. Opt. Soc. Am. B **28**(1), 28–36 (2011).

1. Introduction

The quantum phenomenon of electromagnetically induced transparency (EIT) has been a subject of intensive investigations in recent years due to the EIT-associated features of strong dispersion and slow-light propagation within the transparency (spectral) window [1], promising a variety of potential applications, e.g. in nonlinear mixing and optical storage. However, there are several specific and strict restrictions on the realization of the original EIT (based on the quantum interference of atomic resonances), making the experimental realization of it rather challenging. Recently, a number of classical configurations have been suggested for the realization of EIT-like transmission under less demanding experimental conditions, including coupled dielectric resonators [2,3], metamaterial-induced transparency [4,5] and phase-coupled plasmon-induced transparency [6]. Among these approaches, on-chip photonic analogues of EIT in integrated photonic circuits are of special interest because potential EIT applications can be realized with guided optical devices, introducing novel functionalities into optical integrated circuits. Experimental waveguide-based realization of EIT-like transmission was reported using coupled Si ring resonators, featuring however quite large footprints of hundreds of square microns [3]. Plasmonic devices are more promising in constructing structures with smaller sizes because of their inherent property of strong field confinement. Two metal stripes (different in length) on top of a Si waveguide were suggested to be used as phase-coupled surface plasmon resonators that would ensure EIT-like transmission, resulting in considerably smaller footprints of $\sim\mu m^2$ [6].

It should be noted that the phenomenon of EIT can be considered using two alternative ways: as resulting from the destructive interference between two pathways involving the *bare*, dipole-allowed and metastable, states or, *equivalently*, the doublet of *dressed* states (created by the strong pump radiation) representing two closely spaced resonances decaying to the same continuum [1,7]. While these two physical pictures are equivalent when dealing with the EIT in atomic systems, their realization with classical systems, whose responses are determined by their configurations and *not* electromagnetically induced as in the EIT, *depends* on the EIT mechanism that is imitated [8]. The first (bare-state) picture suggests employing radiative (coupled to a bus waveguide) and subradiant (not coupled to the waveguide) resonators that are mutually coupled by being closely placed [2]. Alternatively viewed, the EIT is achieved due to the cancelation of opposite contributions from two detuned resonances, which are equally spaced but with opposite signs of detuning from the probe frequency (with the detuning being close to the resonance linewidth), due to the Fano-like interference of the decay channels [7]. Consequently, the second (dressed-state) picture suggests using *detuned* resonators that are both coupled to a bus waveguide [3, 6]. In the latter realizations, however, the two detuned resonators were separated by an integer number of mode wavelengths because of the design constraints [3, 6], but such a separation is, in principle, not required for realization of EIT-like behavior.

2. Aperture-coupled Fabry-Perot resonators in MIM waveguides

In this paper, we demonstrate that on-chip EIT-like transmission can be realized with detuned aperture-side-coupled Fabry-Perot resonators (FPRs) in MIM waveguides. MIM waveguides utilize gap surface plasmons allowing extremely tight mode confinement with moderate propagation loss [9], and are thereby especially suitable for deep subwavelength photonic integration. Various plasmonic waveguides of the MIM type have been experimentally investigated, including V-groove channel plasmon-polariton waveguides [10] and plasmonic slot waveguides [11]. When MIM waveguides are terminated within a metal background, the reflectivity at the end is quite high ($\approx$1) due to the small skin depth of metals in optical regime,

#140919 - $15.00 USD Received 10 Jan 2011; revised 26 Jan 2011; accepted 30 Jan 2011; published 3 Feb 2011

which makes MIM waveguides ideal candidates for FPRs. FPRs with ultra-compact lateral dimension and ultra-short lengths can then be constructed, which lead to FPRs with ultra-small footprints. The length of the FPRs can be estimated with the following equation:

$$\mathrm{Re}(k_{MIM})L = m\pi \tag{1}$$

where $\mathrm{Re}(k_{MIM})$ is real part of the propagation constant k_{MIM} of the gap surface plasmon mode in the MIM waveguide, L is the length of the FPR and m is an integer, which is the resonance mode order of the FPR. When the width of the MIM waveguide is not too small, k_{MIM} can be further approximated as [12]:

$$k_{MIM} = k_0\sqrt{\varepsilon_d + \frac{2\varepsilon_d\sqrt{\varepsilon_d - \varepsilon_m}}{k_0 w(-\varepsilon_m)}} \tag{2}$$

in which k_o is the optical wave vector in vacuum, w is the width of the MIM waveguide and ε_m and ε_d are the dielectric constants of the metal and insulator respectively.

Note that, due to the tight mode confinement in MIM waveguides, resonator excitation via evanescent coupling between adjacent MIM waveguides becomes inefficient, when the gap between the bus and resonator waveguides is large enough for practical experimental processing [13]. Aperture coupling was proposed to realize efficient coupling without increasing the waveguide-resonator interaction length and, thereby, ring resonators with high extinction ratios and low modal volumes [14] can be achieved. Here, the aperture-coupling scheme is applied to the FPR excitation.

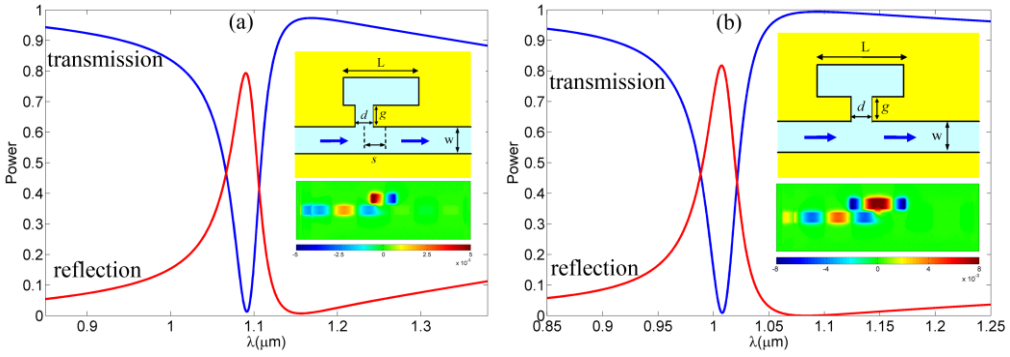

Fig. 1. Transmission and reflection spectra for an aperture-coupled FPR with length L being 300nm (a) and 600nm (b); In both figures, upper Inset is the schematic figure of the structure and lower inset shows magnetic field at resonance.

We start with the consideration of individual MIM-based FPRs utilizing the lowest cavity mode supported in the FPR, i.e. $m = 1$ in Eq [1]. The upper inset in Fig. 1(a) shows the schematic figure for the aperture-coupled FPR, where the background material in yellow is silver, whose permittivity is described by the Drude model $\varepsilon_r = \varepsilon_\infty - \omega_p^2/(\omega^2 + j\gamma\omega)$, with $\varepsilon_\infty = 3.7$, $\omega_p = 9.1$eV and $\gamma = 0.018$eV (parameters obtained by fitting the experimental data [15] at the infrared frequencies). The insulator index is assumed to be 1.45 and the width w for both the bus waveguide and the FPR is 100nm. The gap g between the waveguide and the resonator is 50nm, which allows one to easily make the structure with state-of-the art nanofabrication facilities, and this value is assumed to be constant throughout this paper. Note that the magnetic field in the lowest mode is anti-symmetric along the central plane of the FPR, while the magnetic field into the FPR due to the aperture is symmetric. In order to excite this mode, one has to shift the

#140919 - $15.00 USD Received 10 Jan 2011; revised 26 Jan 2011; accepted 30 Jan 2011; published 3 Feb 2011

aperture (over a distance *s*) away from the FPR center. The finite-difference time-domain (FDTD) method with fast Fourier transform is used to obtain the spectral response of the FPR. The transmission and reflection spectra, when the FPR length *L* is 300nm and the aperture (width *d* = 60nm) is 50nm away from the center of the FPR, are shown in Fig. 1(a). One can see that a strong resonance appears at the wavelength around 1.089μm with a high transmission extinction ratio (≈20dB). The quality factor at the resonant wavelength is not quite large due to the intrinsic loss in the FPR, as well as the fast decaying rate of power from the FPR to the bus waveguide. The latter can be simply adjusted by changing the aperture width *d*. Note that the transmission spectrum suffers from a much lower extinction ratio in this spectral range when there is no aperture (*d* = 0) and the gap *g* is 50nm because of the weak evanescent coupling. The magnetic field in the structure at the resonance is shown as the lower inset in Fig. 1(a), from which we can see that a strong cavity mode with one magnetic field node is formed in the FPR.

For the resonance wavelength of 1.089μm, with Eq [2]. we can calculate the FPR length and find it to be 311nm, which is quite close to the value of 300nm that we use in the FDTD simulation. The small discrepancy can be attributed to the difference between the approximation of k_{MIM} and its exact value for the gap width of 100nm, the additional phase introduced by the aperture which is not taken into account in Eq [1], as well as some numerical errors in the FDTD simulations. However, we note that Eq [1]. can still provide a good estimation of the FPR length and thus can be used to roughly design the FPR. We can also use the 2nd order FPR mode, whose magnetic field is symmetric along the central plane of FPR and then the aperture can be placed at the center of the resonator. The transmission and reflection spectrums in this case where FPR length is 600nm, and aperture width *d* = 50nm are shown in Fig. 0.1(b). One can see that comparable results to Fig. 1(a) are achieved and the lower inset of Fig. 1(b) clearly shows the characteristic field distribution of second order mode.

3. Plasmon-induced-transparency with aperture-coupled FPRs

We further found that, when two aperture-coupled FPRs with slightly different resonant frequencies are placed on the opposite side of the bus waveguide, the EIT-like behavior shows up in transmission spectra (Fig. 2). Detuned FPRs (DFPRs) can be realized by choosing different geometrical parameters. Here, for simplicity, we consider DFPRs with different FPR lengths while keeping their width the same. We put the two apertures away with the same distance *s* from the center of the DFPR [see inset in Fig. 2(a)]. Numerical results, for the DFPR transmission spectra with one FPR length L_1 = 300nm while the length L_2 of the other FPR is 310nm/320nm, are shown in Fig. 2(a). The reflection spectra are omitted here for the sake of clarity. One can see that pronounced EIT-like transmission occurs for both cases, with a high-transmission peak appearing in a wide low-transmission band. The peak transmission is higher than 0.75 when the length deviation between the two FPRs is just 10nm, and increases as the detuning of resonant wavelengths becomes larger. The quality factor for the transmission peak corresponding to L_2 = 310nm is about 60, twice of that for a single aperture-coupled FPR. Although the tradeoff between the quality factor and the peak transmission still exists, both of them can be adjusted by changing the aperture width, which in turn changes the coupling coefficient. Detailed investigations over this topic show that the optimal condition for the EIT-like spectrum is the case when the detuning δ of the two transmission-dip wavelengths from the central wavelength λ_0 ($\lambda_1 = \lambda_0 - \delta$, $\lambda_2 = \lambda_0 + \delta$) equals to $0.5\,\Gamma$, where Γ is the width of the transmission dip when there is only one FPR as shown in Fig. 1 with the resonance wavelength around λ_0. This criterion can be used as a guideline for the designing of these kinds of devices. It should be noted, that a similar condition of the detuning to be close to the broadening of two resonances is also found in the dressed-state picture of the EIT for atomic media [1,7] as well as in that realized with plasmonic metamaterials based on detuned electrical dipoles [8].

#140919 - $15.00 USD Received 10 Jan 2011; revised 26 Jan 2011; accepted 30 Jan 2011; published 3 Feb 2011

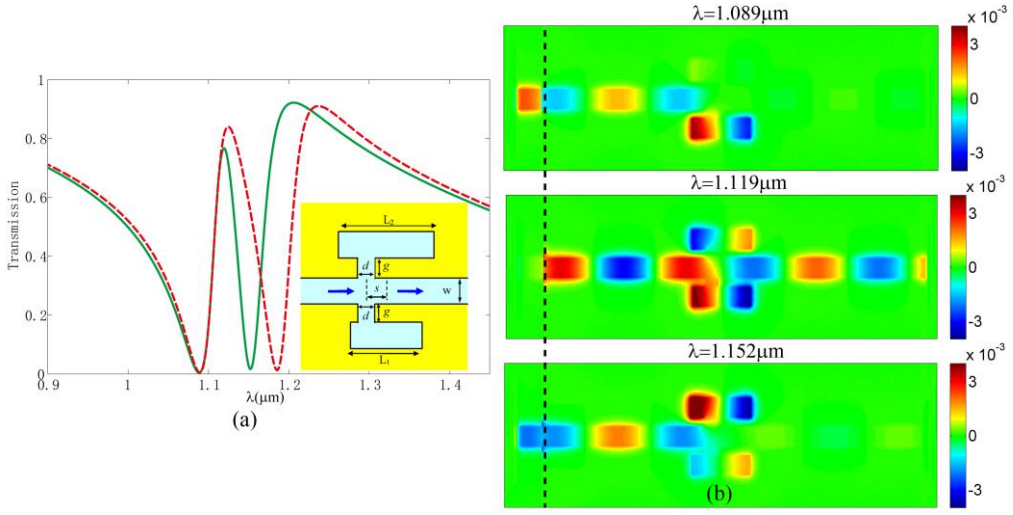

Fig. 2. (a) EIT-like transmission spectra for two FPRs with L_2 equaling to 310nm (solid line), 320nm (dashed line) and L_1 being kept as 300nm. Inset is the schematic figure of the structure. (b) Snapshots of the magnetic field when the light at three different wavelengths is incident into the structure in which L_1 = 300nm and L_2 = 310nm. The black dashed line indicates the incident plane.

To get more insight into the physics of the EIT-like transmission observed, the FPR lengths were kept to be 300nm and 310nm, respectively, while one FPR was shifted along the other in the propagation direction. Simulations for the shift being 0nm, 50nm and 100nm showed that the EIT-like transmission deteriorated with the shift increase, indicating that one cannot gain by introducing the phase-coupling scheme [6], at least not for relatively small FPR displacements. Magnetic field distributions shown in Fig. 2(b) calculated at the two transmission dips (λ_1 = 1.089μm and λ_2 = 1.152μm) and the transmission peak (λ_3 = 1.119μm) for DFPRs with lengths L_1 = 300nm and L_2 = 310nm indicate that the main reason for the occurrence of the transmission peak is related to circumstance that the two FPRs resonate *out of phase* with each other at the intermediate frequency λ_3. It is the destructive interference between the electromagnetic fields in the two FPRs, which allows the incident light to propagate through the structure uninhibited. Judging from Babinet's principle, we also believe that these FPRs with lengths smaller to the resonant wavelengths can be regarded as slot dipole antennas. Thus the DFPR configuration is similar to the case of detuned electrical dipoles [8,16], and the EIT-like transmission can be attributed to the interference between the two detuned slot dipoles, similar to what happens in the metamaterial-induced transparency. At the same time, the coupling is mediated by the bus waveguide between the two FPRs and enhanced with the two apertures. Also note in Fig. 2(b) that for λ_1 = 1.089μm and λ_2 = 1.152μm large magnetic fields exist on the left side of the incident plane which indicates large reflections while this is not true for λ_3 = 1.119μm.

#140919 - $15.00 USD Received 10 Jan 2011; revised 26 Jan 2011; accepted 30 Jan 2011; published 3 Feb 2011

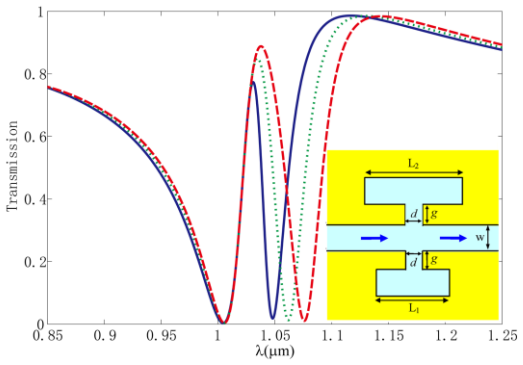

Fig. 3. EIT-like transmission spectra for two FPRs with L_2 equaling to 610nm (solid line), 620nm (dotted line) and 630nm (dashed line) and L_1 being kept as 600nm. Inset is the schematic figure of the structure and the two apertures are located at the center of the two FPRs.

We further investigated two coupled DFPRs resonating at the 2nd order FPR modes, whose configuration is schematically shown as the inset in Fig. 3. Here, as in Fig. 1(b), the apertures with width d = 50nm should be located at the center of the DFPRs. The transmission spectra, when L_1 is kept at 600nm and L_2 changes from 610 to 630nm, exhibit pronounced EIT-like transmission that is rather similar to that found in the previous case [cf. Figure 2(a) and Fig. 3]. Note that, in both cases, the whole structure is ultracompact with the footprint being smaller than 0.15μm^2 (0.25μm^2) for the DFPRs resonating at the lowest (2nd order) modes, values that can be advantageously compared with those previously reported [3, 6].

Having on-chip EIT-like transmission at hand, the next important issue to be considered is related to the expected phenomenon of slow-light propagation, i.e. to the level of group indexes that can be achieved with these structures. Using the continuous wave excitation in the FDTD simulations, a phase distribution for the magnetic field at a specific wavelength can be obtained throughout the whole structure. The effective phase index n_p at this wavelength can then be calculated by considering the phase difference between the fields at bus waveguide positions before and after the DFPRs. Repeating this procedure, the wavelength-dependent effective phase index in the spectral region of our interest can be determined. The results calculated for both DFPR configurations under consideration are shown in Fig. 4 along with the effective phase index for a straight MIM waveguide obtained (with the same method) and plotted for comparison. One can see that, in both cases, n_p varies rapidly near the transmission peak wavelength, deviating considerably from the MIM effective index. In the domain of normal dispersion, the group index n_g can be calculated according to $n_g(\omega) = n_p(\omega) + \omega dn_p(\omega)/d\omega$ and is found to be up to 26 for the lowest FPR mode and 25 for the 2nd order mode at the wavelengths corresponding to the transmission maxima. The high group index achieved here makes the structure very promising for on-chip applications, e.g. compact delay lines and slow-light components. The bandwidth-delay product estimated with $\Delta f \tau \simeq L\Delta\lambda(n_g - n_{g0})/\lambda_0^2$, where L is the distance between two planes where the phases are used to calculate n_p (and can also be considered as the unit cell length), λ_0 is the wavelength where maximum n_g is achieved, $\Delta\lambda$ is the FWHM of the transparency window and n_{g0} is the group index at λ_0 for the MIM waveguide, is found to be 0.31 and 0.30 at the transmission-peak wavelength, for the two cases respectively. Note that these values are also favorably comparable to the bandwidth-delay product calculated for the waveguide configuration with spatially separated plasmonic resonators [6].

#140919 - $15.00 USD Received 10 Jan 2011; revised 26 Jan 2011; accepted 30 Jan 2011; published 3 Feb 2011

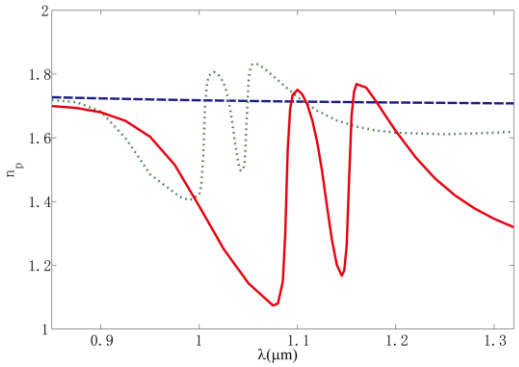

Fig. 4. Wavelength-dependant phase index obtained with the structure in which the solid line is for L_1 = 300nm and L_2 = 310nm while the dotted line is for L_1 = 600nm and L_2 = 610nm; the dashed line is the effective index for the MIM waveguide in this spectral range.

4. Conclusion

In summary, we have demonstrated the on-chip plasmonic EIT analogue with well-pronounced EIT-like transmission in integrated plasmonic devices using aperture- coupled DFPRs realized with MIM waveguides. Group indexes of up to 26(25) can be achieved at near-infrared wavelengths with the footprints being less than 0.15μm^2 (0.25μm^2) for the lowest (2nd order) FPR modes. It is relatively straightforward to employ the same design principle for constructing more sophisticated configurations known from (dielectric-based) photonics, e.g. balanced side-coupled sequences of resonators [17]. We believe that the plasmonic DFPR-based components will find broad applications in nanophotonics and introduce novel functionalities into guided plasmonic circuits, advancing further the subwavelength photonic integration with surface plasmons.

Note added in proof: After submission of our manuscript, we have learned about simulations demonstrating the EIT-like effect of optical transparency achieved in a similar system of side-coupled detuned waveguide-ring resonators [18].

Acknowledgements

This work was supported by the Danish Council for Independent Research (FTP-project No. 09-072949 ANAP).

#140919 - $15.00 USD Received 10 Jan 2011; revised 26 Jan 2011; accepted 30 Jan 2011; published 3 Feb 2011